

Magnetic Storms

Bruce T. Tsurutani
Space Plasma Physics
Jet Propulsion Laboratory, California Institute of Technology
Pasadena, California, 91109

Walter D. Gonzalez
Instituto Nacional Pesquisas Espaciais
Sao Jose dos Campos
San Paulo, Brazil

and

Yosuke Kamide
Solar-Terrestrial Environment Laboratory
Nagoya University, 1 Ionohara 3-13
Toyokawa 442, JAPAN

Abstract

This talk provides a brief summary of the first conference devoted entirely to magnetic storms. Topics cover the relevant phenomena at the sun/corona, propagation of these structures through interplanetary space, the response of the magnetosphere to interaction with these interplanetary structures, the formation of the storm time ring current (in particular the oxygen content of the ring-current), and storm ionospheric effects and ground based effects. The Conference was held in Pasadena, California, at the Jet Propulsion Laboratory, 12-16 February 1996. A complementary summary is provided by Gonzalez et al. in EOS, 1996. The full set of review articles will be published in an AGU monograph and many of the contributed articles will appear in a special section of the Journal of Geophysical Research, Space Physics.

INTRODUCTION

Over 100 talks were presented at the Chapman Conference on Magnetic Storms. The invited talks have been written up and will be published in an AGU monograph. Many of the contributed papers will be published in a special section of the JGR. Because of the limited space for this article, we can only review a few important papers presented at the meeting, and we will not attempt to be thorough in any sense. A complementary review has been written by Gonzalez et al. (1996) for EOS, which has a broader scope than this article. We suggest that the reader go to the original papers for further details. They should be published within months of the appearance of this review.

RESULTS

One of the fundamental new solar observations pertaining to magnetic storms is shown in Figure 1. Hudson has found evidence in Yohkoh soft x-ray images for coronal mass ejections. The "initial" condition is given in the top image. In the bottom image for a later time interval, the complex set of loops has brightened and extended while the region above the loops is darkened. The latter indicates that the mass present in this area has decreased and most probably has been expelled into interplanetary space.

expelled

During solar maximum, when the sun has the most number of sunspots and is the most active, the "fast" coronal mass ejections are related to the most intense magnetic storms. By "fast" we mean having velocities over 500 km s^{-1} . The fast events contain two basic regions where the magnetic fields have intensities $>10 \text{ nT}$ (the typical interplanetary magnetic field is $3\text{--}8 \text{ nT}$). The first is the driver gas region, whose fields can vary from $10\text{--}60 \text{ nT}$. This region is typically low beta, ~ 0.1 . A second region is the compressed sheath speed ahead of the driver gas. The strength of the field in this region depends partly on the strength of the forward shock bounding its anti-solarward extent (the magnetic compression is proportional to the shock Mach number). A schematic of both driver gas and sheath is given in Figure 2.

Table 1 gives the interplanetary requisites for creating an intense magnetic storm at Earth. First, the interplanetary magnetic field must be intense. Secondly, the field direction must be opposite to that of the Earth's magnetopause fields, or southwardly directed. Third, the southwardly directed fields must last for several hours. Statistically these three requisites have been found to occasionally occur during solar ejecta events with above average solar wind speeds ($V_{\text{sw}} > 500 \text{ km/s}$). Although the velocity is a main parameter in the cross-tail electric field [$E = 1/c \vec{V} \times \vec{B}$], the magnitude of solar wind velocity variation is small compared to the variation in B_s . The solar wind speed only varies by a factor of 2-3, while B_s can vary from 0 to 60 nT .

The driver gas sometimes has a significant southward component. These typically occur in what have been called magnetic clouds. The most likely configuration is that of a flux rope, shown in Figure 3. The flux rope configuration has a north-south or south-north orientation. The southward field causes storm main phases through magnetic reconnection, and the northward component, geomagnetic quiet. Only one in six high-speed solar ejecta events have a magnetic cloud configuration leading to a magnetic storm, however. The other 5 out of 6 events have complex field structures. The magnetic tongue configuration of Gold (1962) was recently sought in the ISM-3 data. However, none was found out of 57 solar ejecta events occurring in 1978-1979.

There have been a number of possible mechanisms for southward sheath field orientations. Some of these are shown in Figure 4. We refer the reader back to the original articles. One comment should be made about magnetic field draping [items d), e) and f)]. The main sheath draping mechanism discussed by Midgley and Davis (1963) and Zwan and Wolf

(I 976) are caused by squeezing of plasma out of the ends of the lines of force, leaving a low beta plasma. This is the cause of the "depletion layer" found near the earth's magnetopause. Since total pressure is maintained across the sheath, such field draping can be observed by an increase in the sheath magnetic field strengths (pressure) as the object boundary is approached. This phenomena is quite noticeable in the data of the magnetosheaths of large planetary systems, such as at Jupiter and Saturn, and also at comets. However, the amount of this type of draping is of a much smaller magnitude bounding solar ejects. The field increase is typically less than 20%. Another type of draping gives north-south field components. One mechanism has been proposed by McComas et al. (1989) and another was that proposed by Odstreil (1996) for high-speed interaction with the heliospheric current sheet (HCS). The figures are self-explanatory. It is not known at present how often the latter mechanisms occur, and how geoeffective these are (a large B_z component needs to be created, and the structures need to be large to have long duration fields imposed on the magnetosphere).

The statistics of the occurrence of magnetic storms on solar ejecta and interplanetary shocks are given in Table 2. The statistics for "big" storms with $8 < K_p \leq 9$ (equivalent to $D_{st} \leq -200$ nT) is highly correlated to shocks (from Gosling et al., 1991). This dependence decreases with decreasing storm intensity. The values for storms of intensities ≤ -100 nT, $-100 \text{ nT} \leq D_{st} \leq -50$ nT, and $-80 \text{ nT} \leq D_{st} \leq -30$ nT are given. The bottom panel shows the interplanetary relationship for storms with D_{st} intensities between -100 nT and -50 nT.

Descending Phase of the Solar Cycle

The causes of storms during the descending phase of the solar cycle are different. Polar coronal holes migrate to low latitudes during this phase of the solar cycle. It has been shown by Ulysses that high speed streams of velocity $\sim 750\text{-}800 \text{ km s}^{-1}$ emanate from coronal holes. Since these structures are often long lasting, the streams "corotate" with the solar rotation period of ~ 27 days.

Figure 5 shows an unusual CC K1101 hole of May 14, 1992 taken by Yohkoh soft x-ray instrumentation. This coronal hole (the dark region) appears to go from pole to pole.

An example of a stream interaction with the upstream slow speed stream is shown in Figure 6. The tenuous high-speed stream interacts with a high density low-speed stream

associated with a heliospheric current sheet at ~0600 UT day 177. The interaction forms a compressed region of magnetic fields, called a corotating interaction region (CIR). In this case, the CIR has not formed either forward or reverse shocks at its boundaries, so we call this a proto-CIR. It extends from 00 UT day 177 to 00 UT day 178. Peak field magnitudes reach 20-25 nT.

The geomagnetic activity in D_{ST} has a different signature than that of storms occurring during solar maximum. Because there are rarely forward shocks bounding proto-CIRs at 1 AU, there are no storm sudden impulses (storm sudden commencements). The initial phase (magnetospheric compression) is caused by high density plasma of the ICS plasma sheet impinging upon the magnetosphere. This is considerably different than the physical causes of storm initial phases associated with fast solar ejecta occurring during solar maximum. In this case, the storm main phase is small and highly irregular in profile. This is caused by the irregular B_z structure within the CIRs. Although southward components as large as -15 nT are present, the duration of these intervals are short, not allowing for an intense magnetospheric ring current to develop.

The geomagnetic activity caused by proto-CIRs is given in Table 3. It is noted that intense storms did not occur at all during 1974 due to proto-CIR/magnetospheric interactions. CIRs only produce recurrent, low ($ICMC$) storm activity at best.

Table 4 illustrates that the average value of AE during 1974 is larger (283 nT) than that for either 1979 (221 nT) or 1981 (237 nT), the latter two being solar maximum years. The reason for this is the presence of large amplitude Alfvén waves in the coronal hole streams. Since the 'O' streams (one flowing from the north and one from the south) are present throughout much of 1973-1975, the earth's magnetosphere was continuously bombarded by such field fluctuations. Figure 7 illustrates the Alfvén wave B_z variations and concomitant AE (substorm) increases. Substorms occur with each interplanetary B_z event through the process of magnetic reconnection.

Ring Current

The storm time ring current is dominated by oxygen ions. Figure 8 gives the percent oxygen ion energy density (middle panel) as a function of D_{ST} (bottom panel). The event was recorded by CRRIS on March 23, 1991 and is for the outer ring current ($L = 5-7$).

The percentage of oxygen ion energy density is expected to be even higher in the main portion of the ring current ($L = 2-3$). The figure comes from Daglis (1996).

Figure 9 from Daglis, et al. (1994) demonstrates that oxygen ion upwelling from the ionosphere, also occurs during substorms (left panel). The more intense the substorm, the greater the magnetospheric oxygen energy density. The same relationship is not present for the He^{++} ions.

Hamilton (1996) using AMPTE/CCF ion measurements, has shown that the ring current exhibits a solar cycle dependence. This is shown in Figure 10. From left-to-right, the three panels are the relative ion energy densities for quiet intervals during solar minimum, storm-time intervals during solar minimum, and storm-time intervals during solar maximum. The energy range measured is 1-300 keV/e (the bulk of the ring current) and in the region from $L=3-5$. During solar minimum, hydrogen ions totally dominate. For an average storm intensity of $D_{ST} = -102$ nT, oxygen contributes 20% of the energy density. For the $D_{ST} = -93$ nT storm of January 5, 1989, the O^+ energy density reached 44%. Hamilton (1996) also demonstrated that the solar F10.7 radio emission (a proxy for solar EUV emission) increased from solar minimum to solar maximum (not shown), and therefore he has postulated that the larger ionospheric scale heights at solar maximum "enhances the O^+ contribution to the storm-time ring current".

Frank et al. (1996) has shown that GEOTAIL CPI ion distribution functions have unusual features that contain memory of ion beams coming from the ionosphere-proper or from above-ionospheric heights. Such distributions are given in Figure 11. An interpretive cartoon is shown in Figure 12. One possible interpretation that we mention here is that upwelling oxygen ions get accelerated to 3-5 keV by substorm parallel electric fields. These substorms occur during the storm main phase, and are thus an integral part of the storm dynamics. The ions which flow out to the distant plasmasheet are then subsequently convected inward to low L shells and are energized to 10-300 keV by the storm large scale convection electric field to form the main part of the ring current.

The energy flow in the ionosphere is given in Figure 13, taken from Proelss (1996). The plasma gains a velocity drift due to the penetration of the solar wind $\vec{V} \times \vec{B}$ electric field into the magnetosphere. The $\vec{E} \times \vec{B}$ drift imparts kinetic energy into the exospheric plasma. Plasma-neutral collisions lead to acceleration and formation of neutral winds and also to an

increase into neutral temperature (via collisional heating). Magnetospheric and ionospheric plasma instabilities lead to precipitation of particle energy at ionospheric heights in the auroral zone and to further heating of both the ionized and neutral atoms and molecules.

The density variations at 300 km altitude in auroral regions show significant modifications during storms and substorms. Figure 14 gives a satellite pass during substorm activity. Note that the major constituent N_2 increases in spite of the temperature enhancement. Continuous upwelling will eventually set up a vertical circulation cell of the Hadley type. The upward velocity has to increase in proportion to the decreasing density of the major gas. Since the particle flux of the major gas N_2 is approximately constant with height, this will lead to a depletion or enhancement (depending where) of the minor gas. Note the O and He densities decrease in the Figure.

Magnetic storms also have disastrous consequences for power transformers on the ground. Figure 15 is a picture of a large transformer that was damaged during the March 1989 superstorm (from Kappenman, 1996). The nuclear plant transformer was one phase of a 1200 MVA bank that exists on the Delaware river in New Jersey. The loss of production from the plant cost customers up to \$400,000 per day during the 6 week outage.

Figure 16 shows the internal damage of this transformer. Although the large copper strands *were* rated at 3000 amperes, the saturation of the steel core created stray flux that created hot spots and the consequential meltdown.

Minnesota Power performed statistical analyses of transformer failures across the U.S. between 1968 to 1991 and found that the failure rates were 48 to 60% higher in the upper midwest and New England areas in comparison to the rest of the U.S. The mechanism for the strong induced current causing the damage is shown in Figure 17. The intense ionospheric electrojet currents (at ~100 km altitude) descend to lower latitudes during storm conditions. Large currents are induced in the conducting sea water. When adjacent power systems on land are located over high resistivity igneous rock, the induced currents enter and exit power systems through the transformer neutral grounding points.

Acknowledgments. We wish to thank I. Daglis, L. L. Frank, D. Hamilton, H. Hudson, B. Jackson, J. Kappenman and G. Proelss for the use of their figures. The Magnetic Storm meeting was held by the American Geophysical Union at the Jet Propulsion Laboratory, Pasadena, California. Portions of this work were performed at the Jet

Propulsion Laboratory, California Institute of Technology, Pasadena, under contract with the National Aeronautics and Space Administration.

REFERENCES

- Daglis, I. A., S. Livi, E. T. Sarris and B. Wilken, Energy density of ionospheric and solar wind origin ions in the near-Earth magnetotail during substorms, J. Geophys. Res., 99, 5691, 1994.
- Daglis, I. A., The role of magnetospheric-ionospheric coupling in magnetic storm dynamics, submitted to Magnetic Storms, edited by B. T. Tsurutani, W. D. Gonzalez and Y. Kamide, AGU Mon., Wash. D.C., 1996.
- Frank, J. A., W. R. Paterson, K. L. Ackerson, S. Kokubun, and T. Yamamoto, Plasma velocity distributions in the near-Earth plasma sheet: A first look with the GEOTAIL spacecraft, J. Geophys. Res., in press, 1996.
- Gold, J., Magnetic Storms, Space Sci. Rev., 1, 100, 1962.
- Gonzalez, W. D., Y. Kamide and B. T. Tsurutani, Chapman Conference on Magnetic Storms, to appear in EOS, 1996.
- Gosling, J. T., D. J. McComas, J. L. Phillips, and S. J. Bame, Geomagnetic activity associated with Earth passage of interplanetary shock disturbances and coronal mass ejections, J. Geophys. Res., 96, 7831, 1991.
- Hamilton, D. C. and M. E. Greenspan, Average storm-time ring current ion spectra near solar minimum, submitted to J. Geophys. Res., 1996.
- Hudson, H. S., The solar antecedents of magnetic storms, submitted to Magnetic Storms, ed. by B. T. Tsurutani, W. D. Gonzalez and Y. Kamide, AGU Mon., Wash. D. C., 1996.

- McComas, D. J., J. T. Gosling, S. J. Bame, E. J. Smith and H. V. Cane, A test of magnetic field draping induced B_z perturbations ahead of fast coronal mass ejecta, J. Geophys. Res., 94, 1465, 1989.
- Midgley, J. F. and L. Davis Jr., Calculation by a moment technique of the perturbation of the geomagnetic field by the solar wind, J. Geophys. Res., 68, 5111, 1963.
- Odstreil, D., Numerical simulation of interplanetary plasma clouds propagating along the heliospheric plasma sheet, Astrophys. Lett. Comm., in press, 1996.
- Proelss, G. W., Magnetic storms associated perturbation of the upper atmosphere, submitted to Magnetic Storms, edited by B. T. Tsurutani, W. D. Gonzalez and Y. Kamide, AGU Mon., Wash. D.C., 1996.
- Tsurutani, B. T., W. D. Gonzalez, A. L. C. Gonzalez, F. Tang, J. K. Arballo, and M. Okada, Interplanetary origin of geomagnetic activity in the declining phase of the solar cycle, J. Geophys. Res., 100, 21717, 1995.
- Zwan, B. J. and R. A. Wolf, Depletion of the solar wind plasma near a planetary boundary, J. Geophys. Res., 81, 1636, 1976.

-
- Intense Interplanetary Magnetic Fields (IMFs)
 - Intense IMF B_s Values
 - Long Duration (hours) of B_s
 - Above Average Solar Wind Velocity (V_{sw})
-

Table 1

ISEE-3 Statistics During Solar Maximum

Storm Type	No. of Events	Definition	Association with Shocks
"Big"		$D_{ST} \leq -200 \text{ nT}$	100%
Intense	10	$D_{ST} < -100 \text{ nT}$	80%
Moderate	40	$-100 \text{ nT} \leq D_{ST} \leq -50 \text{ nT}$	45%?
Small	62	$-50 \text{ nT} \leq D_{ST} \leq -30 \text{ nT}$	24%

Interplanetary Association of Moderate ($-100 \text{ nT} \leq D_{ST} \leq -50 \text{ nT}$) Storms ISEE-3 (Aug 1978- Dec 1979)

40% Shocks

23% High-speed streams without shocks

17% High-Low speed stream interactions

10% NCDEs

10% Other (including Alfvénic fluctuations)

Geoeffectiveness of Proto-C Rs IMP-8 Days 1-241, 1974

We I-developed streams ($V_{sw} = 600-850 \text{ km s}^{-1}$)		
ntense storms	$(D_{ST} < -100 \text{ nT})$	0%
Moderate storms	$(-100 \text{ nT} \leq D_{ST} < -50 \text{ nT})$	29%
Small storms	$(-50 \text{ nT} \leq D_{ST} < -30 \text{ nT})$	29%
Negligible storm activity	$(-30 \text{ nT} \leq D_{ST})$	41%

Geomagnetic Activity Can be Higher During Solar Minimum Than During Solar Maximum

Solar Minimum	Solar Maximum
$\overline{AE}_{1973} = 247 \text{ nT}$ $\overline{D}_{ST, 1973} = -14 \text{ nT}$	$\overline{AE}_{1979} = 221 \text{ nT}$ $\overline{D}_{ST, 1979} = -16 \text{ nT}$
$\overline{AE}_{1974} = 283 \text{ nT}$ $\overline{D}_{ST, 1974} = -14 \text{ nT}$	$\overline{AE}_{1980} = 180 \text{ nT}$ $\overline{D}_{ST, 1980} = -11 \text{ nT}$
$\overline{AE}_{1975} = 224 \text{ nT}$ $\overline{D}_{ST, 1975} = -10 \text{ nT}$	$\overline{AE}_{1981} = 237 \text{ nT}$ $\overline{D}_{ST, 1981} = -24 \text{ nT}$

Table 4

FIGURE CAPTIONS

Figure 1. Evidence of a coronal mass ejection in Yohkoh soft-x-rays.

Figure 2. A schematic of the interplanetary features due to a solar ejecta event.

Figure 3. Driver gas magnetic field configurations.

Figure 4. Sheath magnetic field configurations.

Figure 5. An unusual coronal hole imaged in soft x-rays. Courtesy of B. Jackson.

Figure 6. Corotating stream interaction with a HCS plasmashet, and the formation of a proto-CIR.

Figure 7. The relationship between the B_s portion of Alfvén waves and AE .

Figure 8. The oxygen ion ring-current energy density as a function of storm-time D_{ST} .

Figure 9. The Oxygen and He^{++} ion energy densities as a function of AE .

Figure 10. Ring-current ion energy densities for solar-minimum quiet, solar-minimum storm conditions and solar-maxima storm conditions.

Figure 11. GEOTAIL, CPI ion distribution functions.

Figure 12. An interpretive schematic of the ion distributions functions shown in Figure 11.

Figure 13. Ionospheric/upper atmospheric plasma/neutral processes occurring during storms.

Figure 14. Velocity, temperature and density variations at 300 km altitude at auroral latitudes during substorms.

Figure 15. A transformer for a New Jersey nuclear power plant that was damaged in the March 1989 superstorm.

Figure 16. Internal damage of the transformer.

Figure 17. The coupling of storm-time ionospheric currents and power lines.

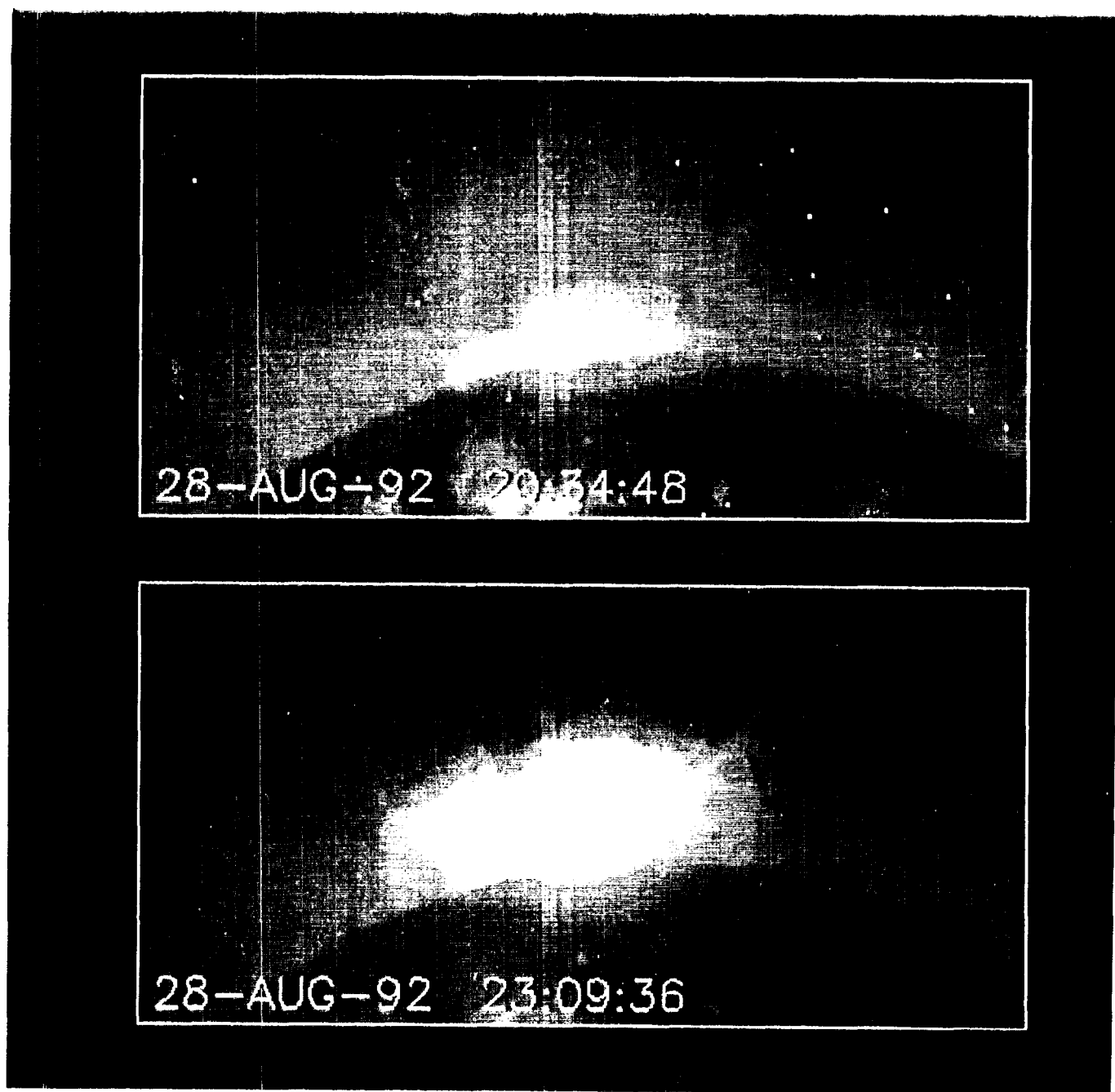
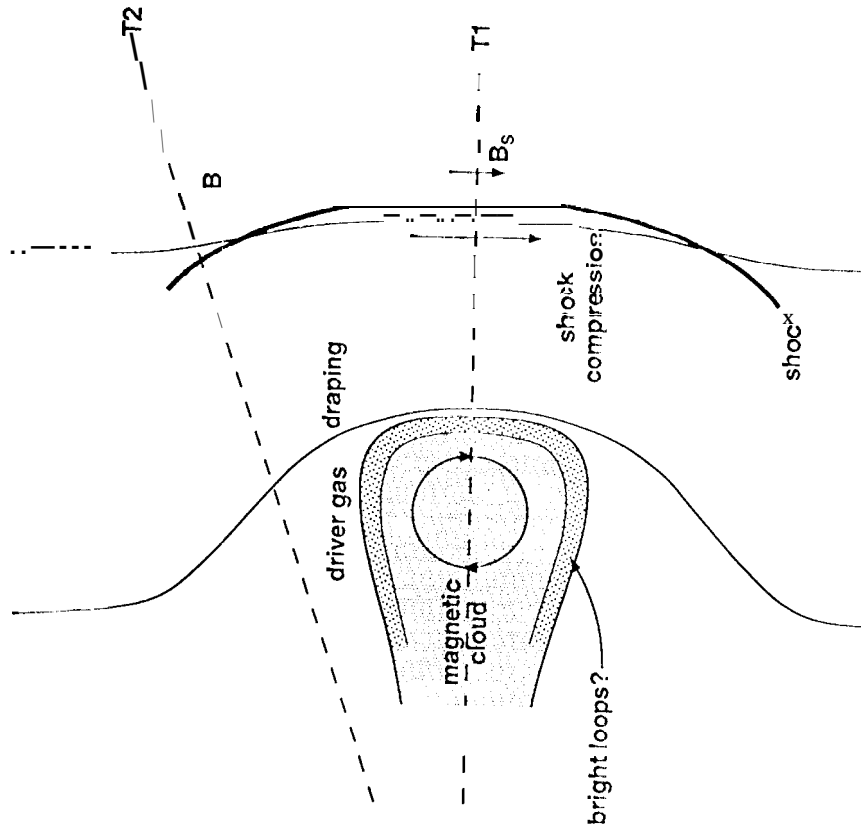


Figure 1

Solar Maximum: Types of Large B Fields

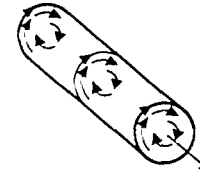


- T1: Crossing at the center of the shock/magnetic cloud structure
- T2: Crossing off-center of the shock/magnetic cloud structure (missing the driver gas)

Figure 2

Driver Gas Fields

a) First version of
magnetic clouds
Klein and Burlaga, 1982



b) Fluxropes
Burlaga et al., 1990



c) Magnetic tongues
Gold, 1962

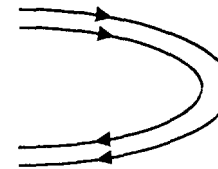


Figure 3

Sheath Fields

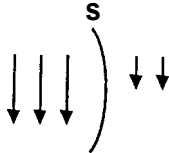
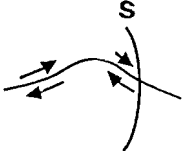
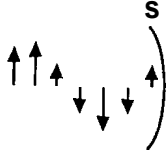
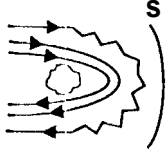
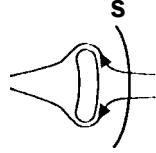
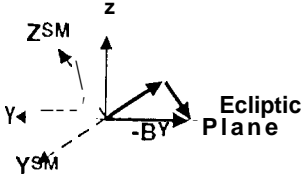
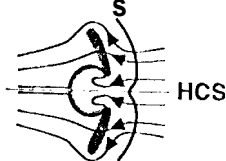
- | | |
|--|--|
| <p>a) Shocked southward fields
Tsurutani et al., 1988a</p> |  |
| <p>b) Heliospheric current sheets
Tsurutani et al., 1984</p> |  |
| <p>c) Alfvén waves and turbulence
Tsurutani et al., 1995b</p> |  |
| <p>d) Draped magnetic fields
Midgley and Davis, 1963
Zwan and Wolf, 1976</p> |  |
| <p>e) Field draping
McComas et al., 1989</p> |  |
| <p>f) Equinoctial B_y effect
Russell and McPherron, 1973</p> |  |
| <p>g) Fast stream-HCS plasmasheet interaction
Odstrčil, 1996</p> |  |

Figure 4

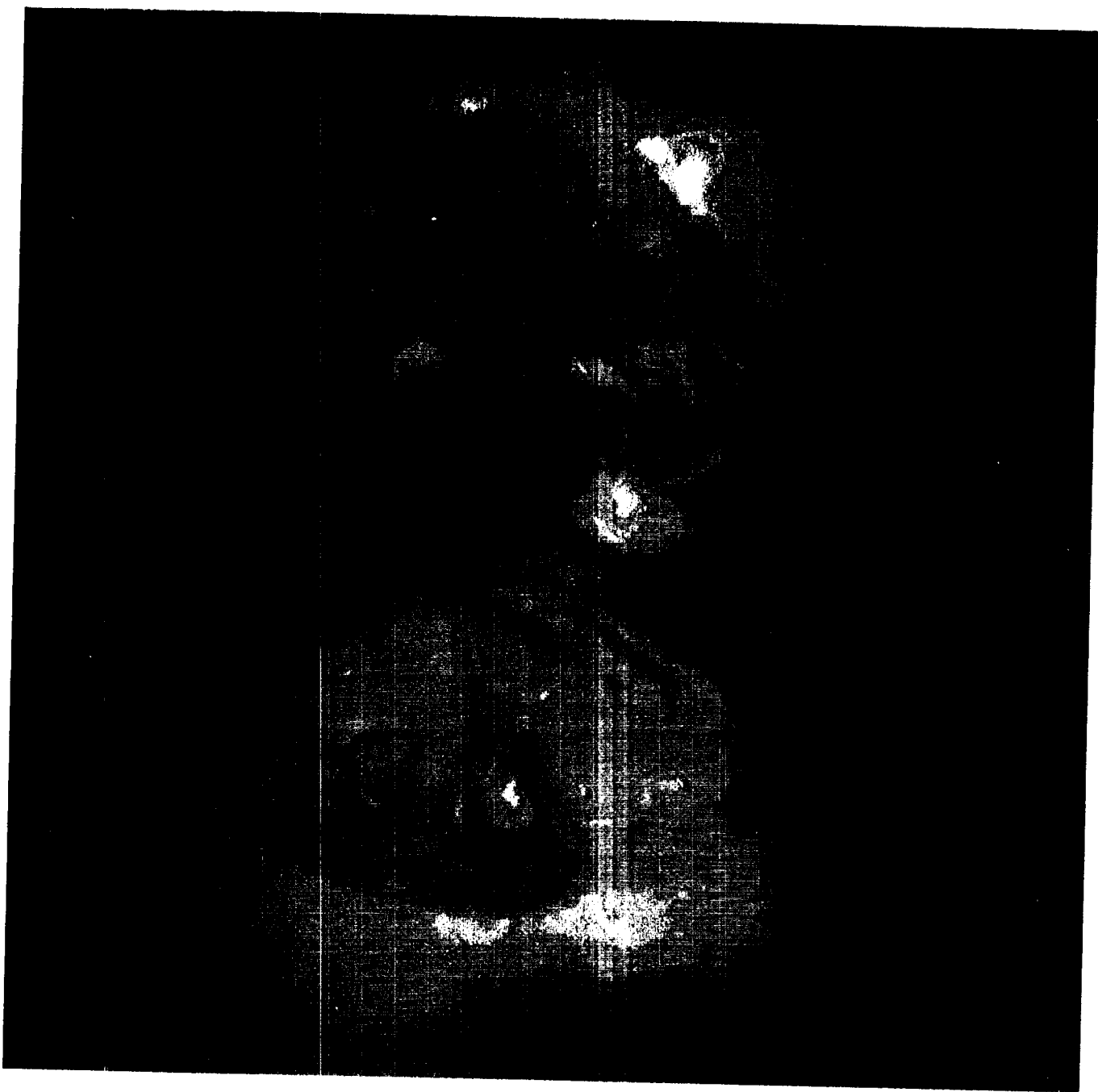


Figure 5

25-28 JUNE, 1974
DAY 176-179

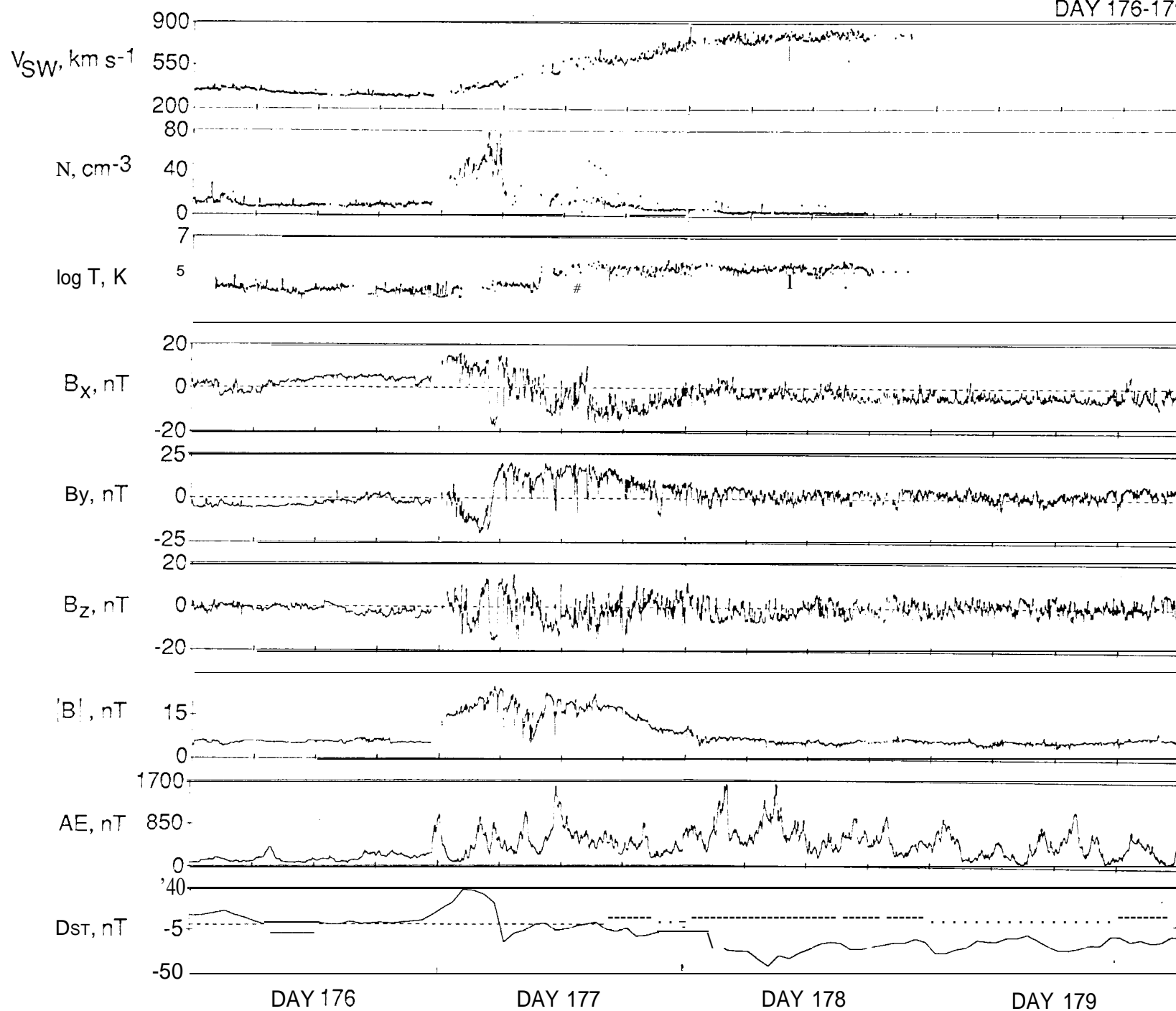


Figure 6

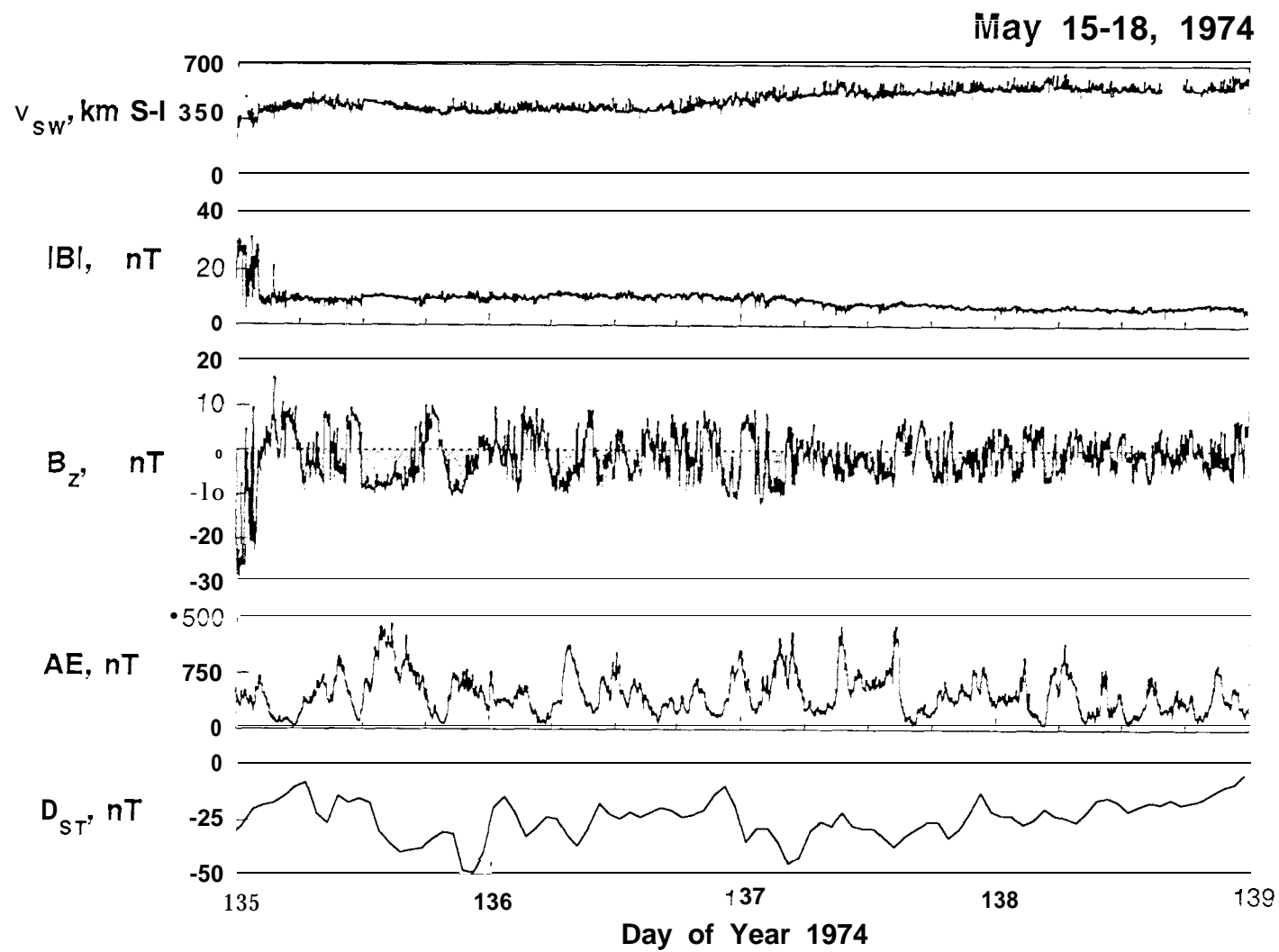


Figure 7

CRRES orbits 0586-0592

MICS/MPAe-AC-UoB-RAL

Date: 23.03.91 D(')Y: 08?

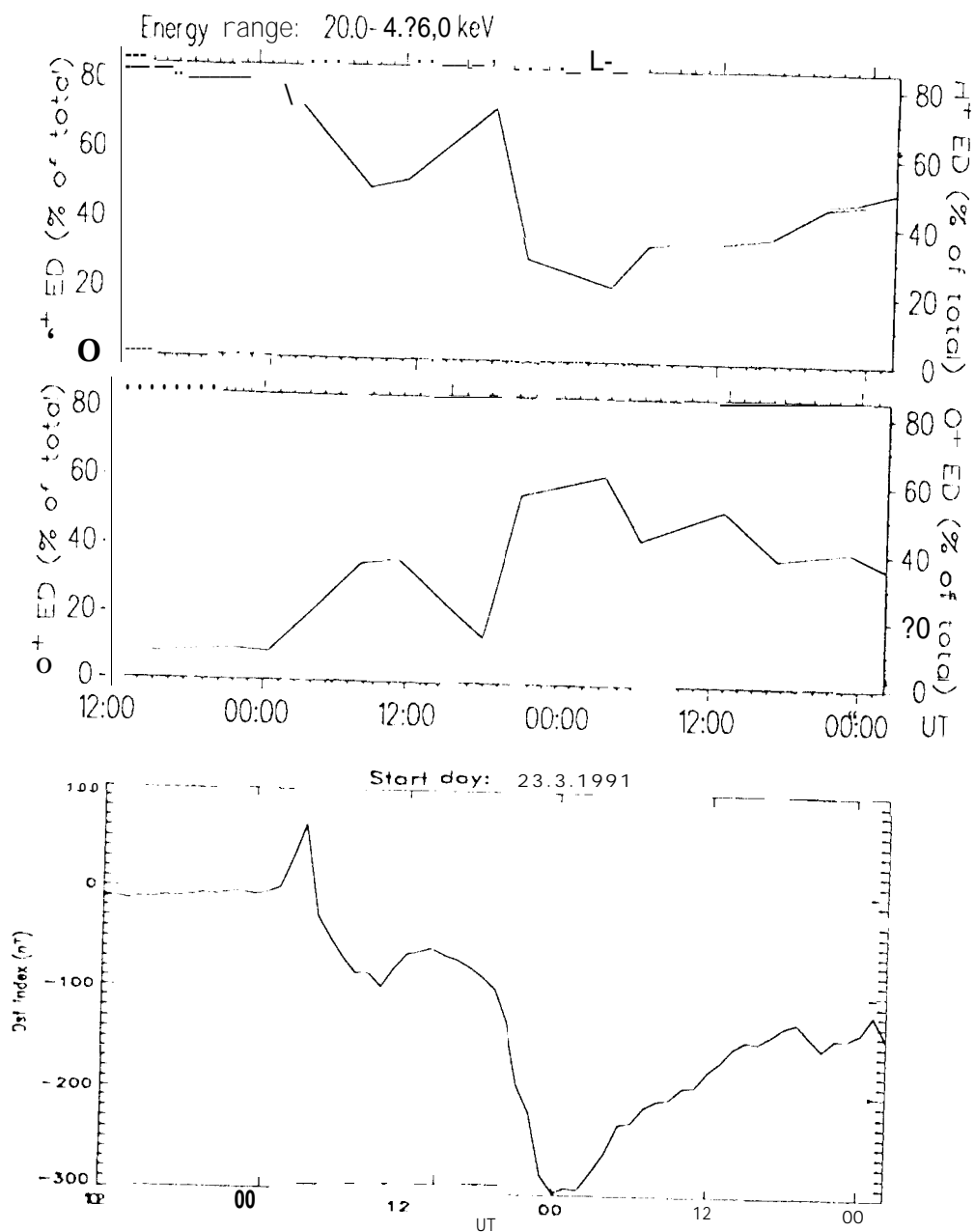
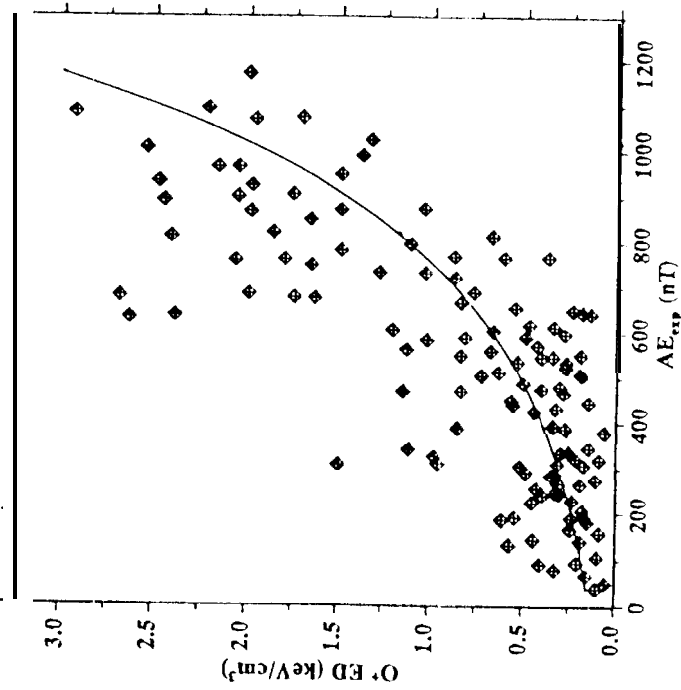
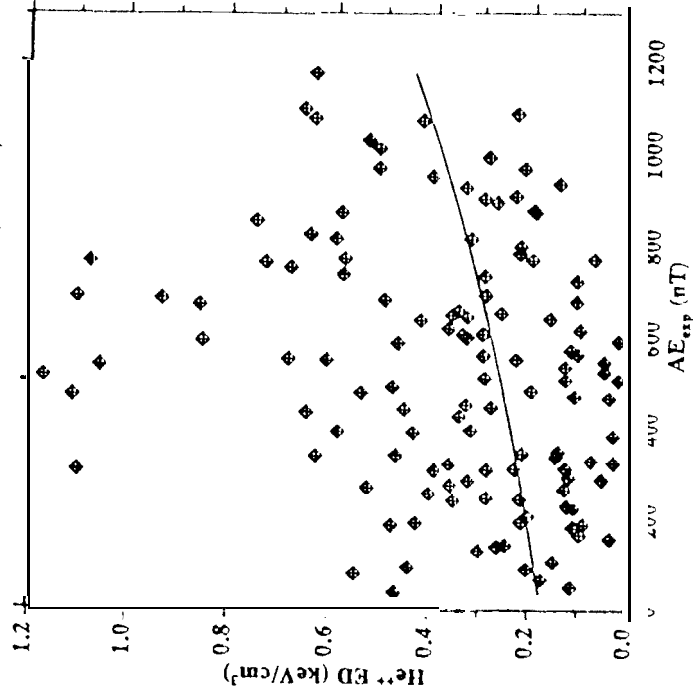


Figure 8

Ion energy density at substorm expansion-phase
 AMPTE/CCE - CHEM spectrometer (126 events)
 Exponential fit: $b=2.63 \times 10^{-3}$, $a=0.14$, $r=0.75$, $F=155.50$



Ion energy density at substorm expansion-phase
 AMPTE/CCE - CHEM spectrometer (126 events)
 Exponential fit: $b=0.79 \times 10^{-3}$, $a=0.17$, $r=0.25$, $F=8.24$



Daglis et al. 1994

Figure 9

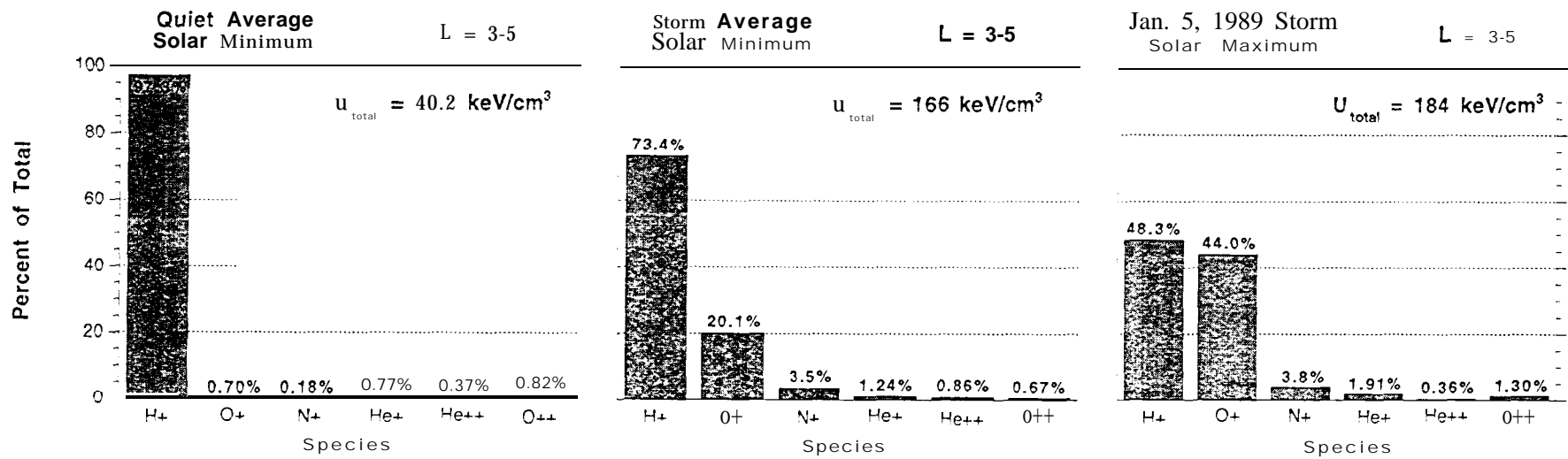


Figure 10

GEOTAIL

HOT PLASMA ANALYZER (CPI-HP)

23 MAY 1995

PROTON PITCH ANGLE DISTRIBUTIONS

$f(\vec{V})$, S^3/CM^6

10^{-25}

10^{-26}

10^{-27}

10^{-27}

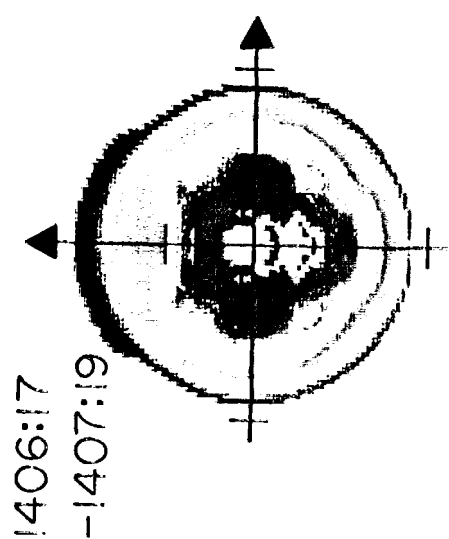
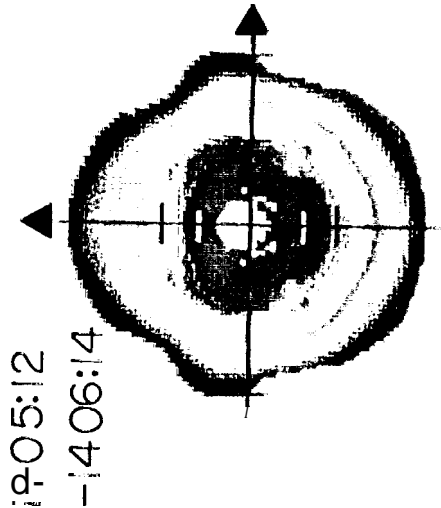
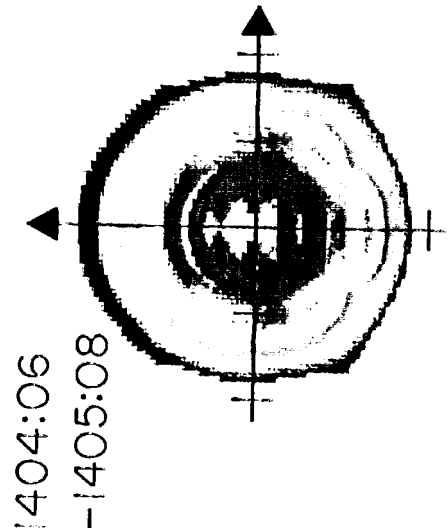
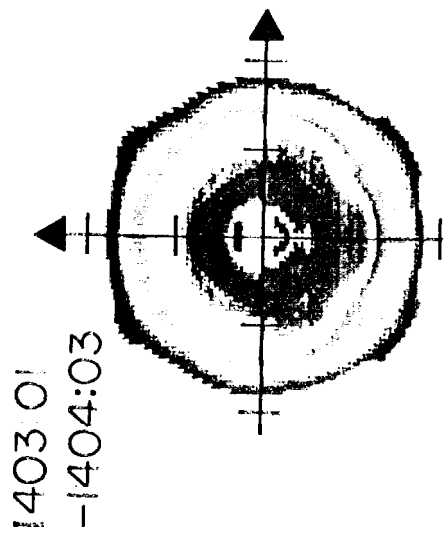
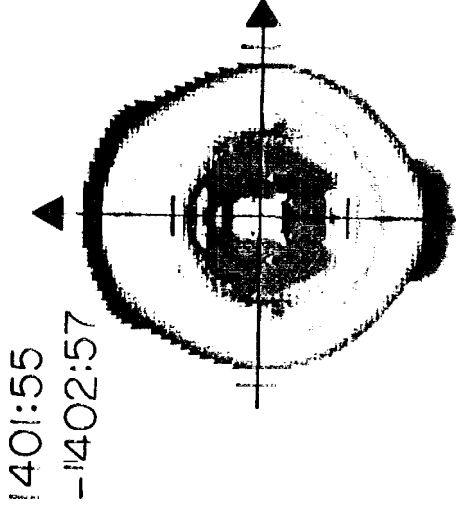
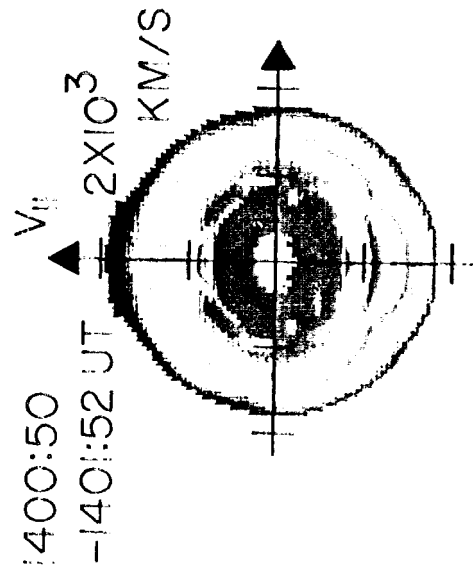


Figure 11

INTERPRETIVE DIAGRAM FOR PLASMA PHENOMENA
OBSERVED IN THE NEAR-EARTH PLASMA SHEET ($\sim 10 R_E$)
WITH THE GEOTAIL SPACECRAFT

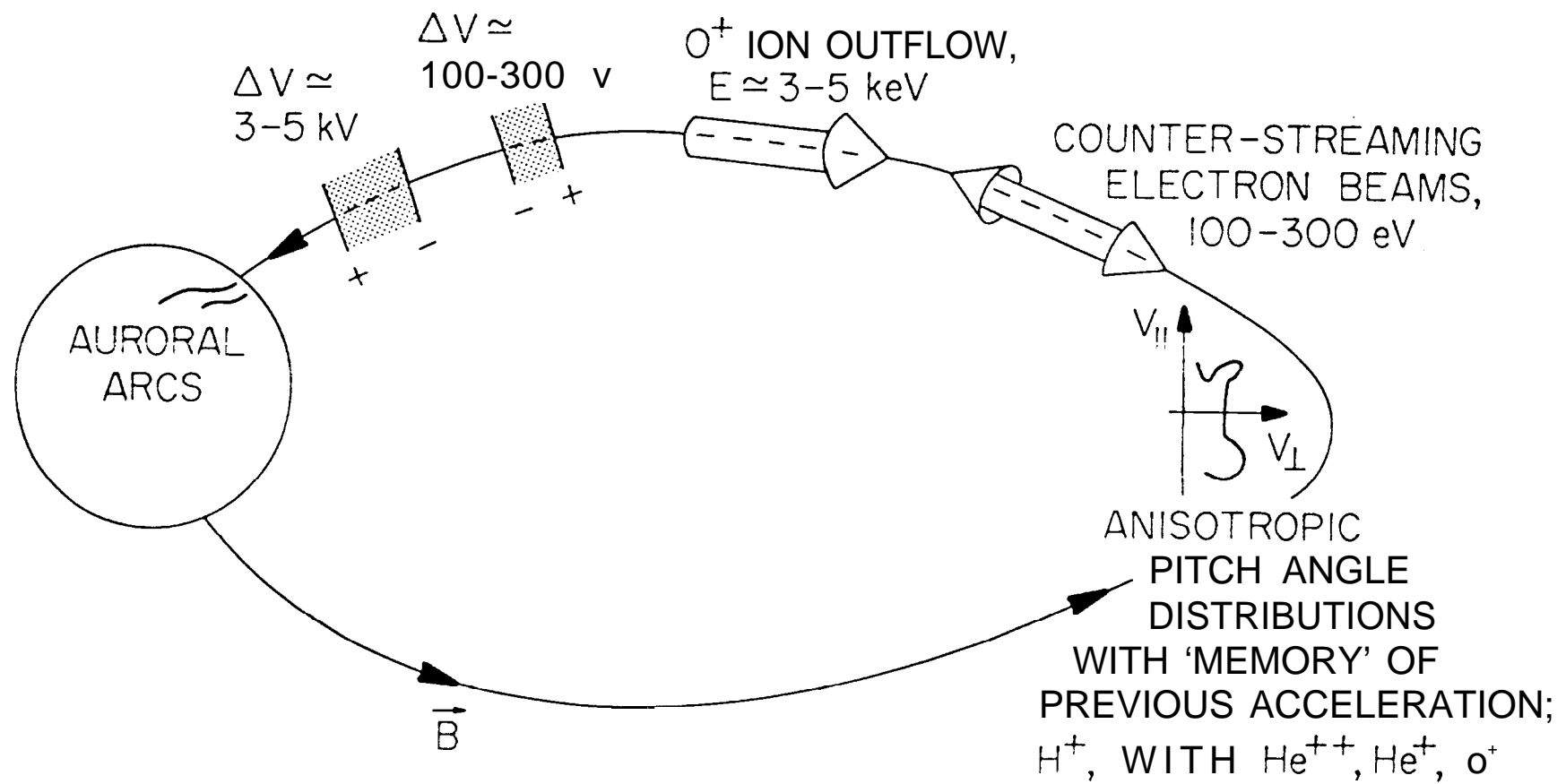


Figure 12

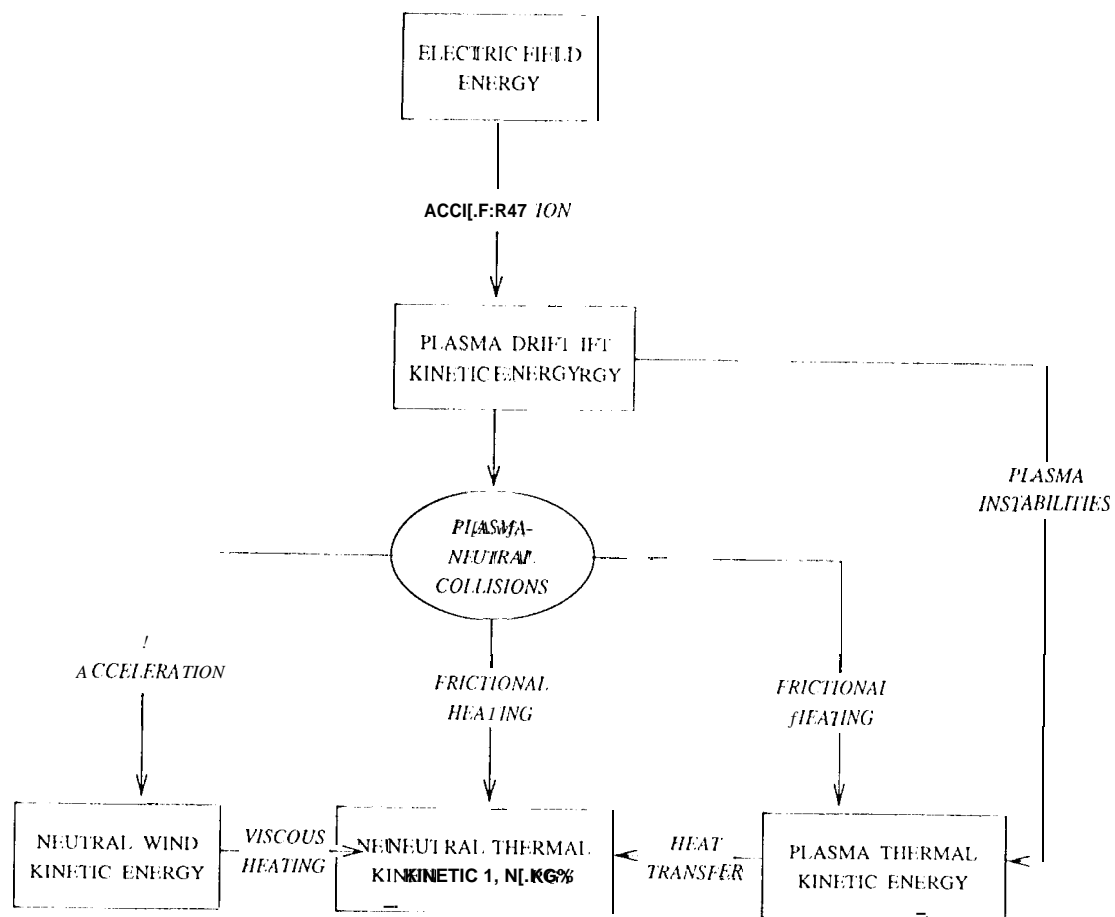


Figure 13

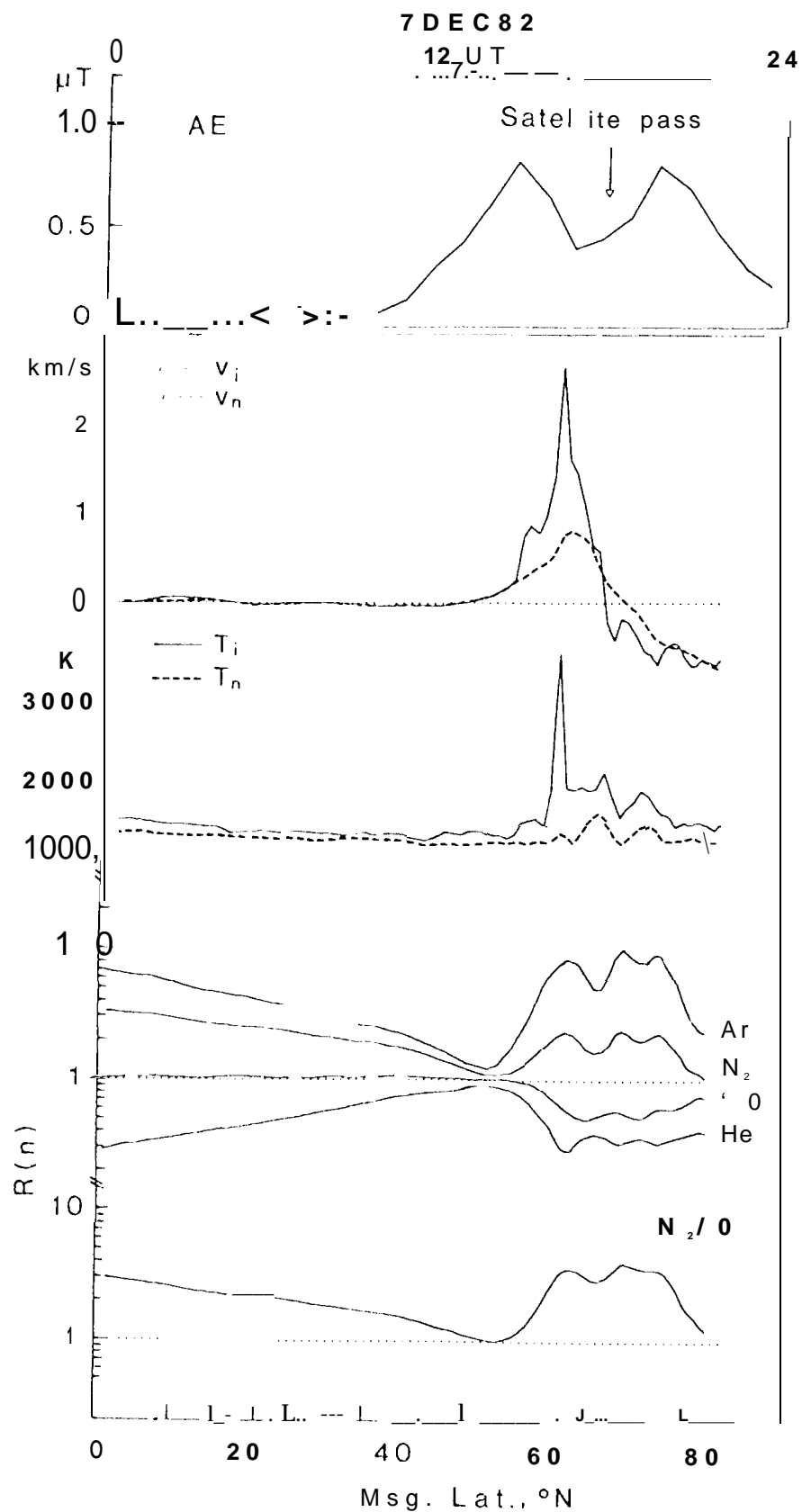


Figure 14

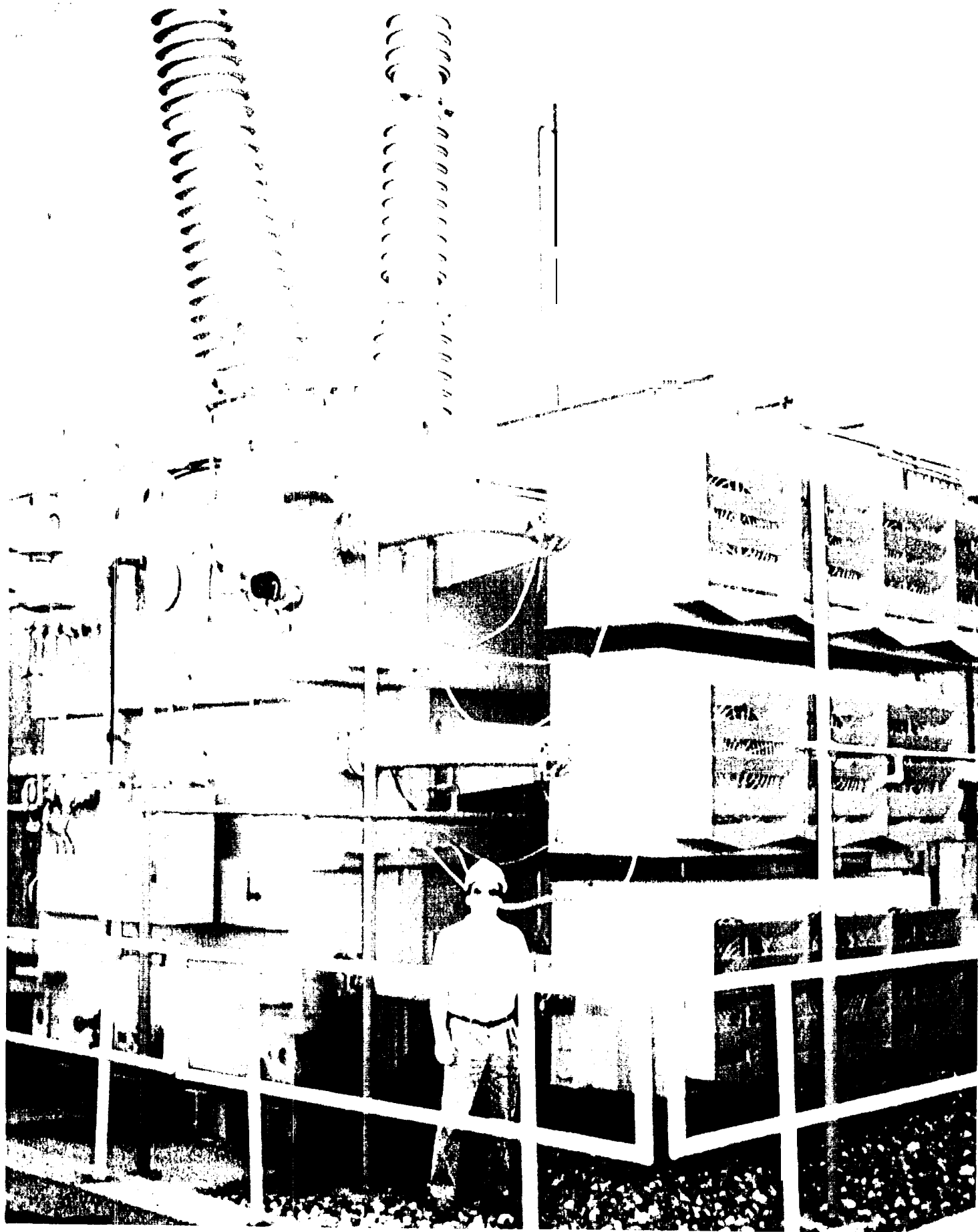


Figure 15

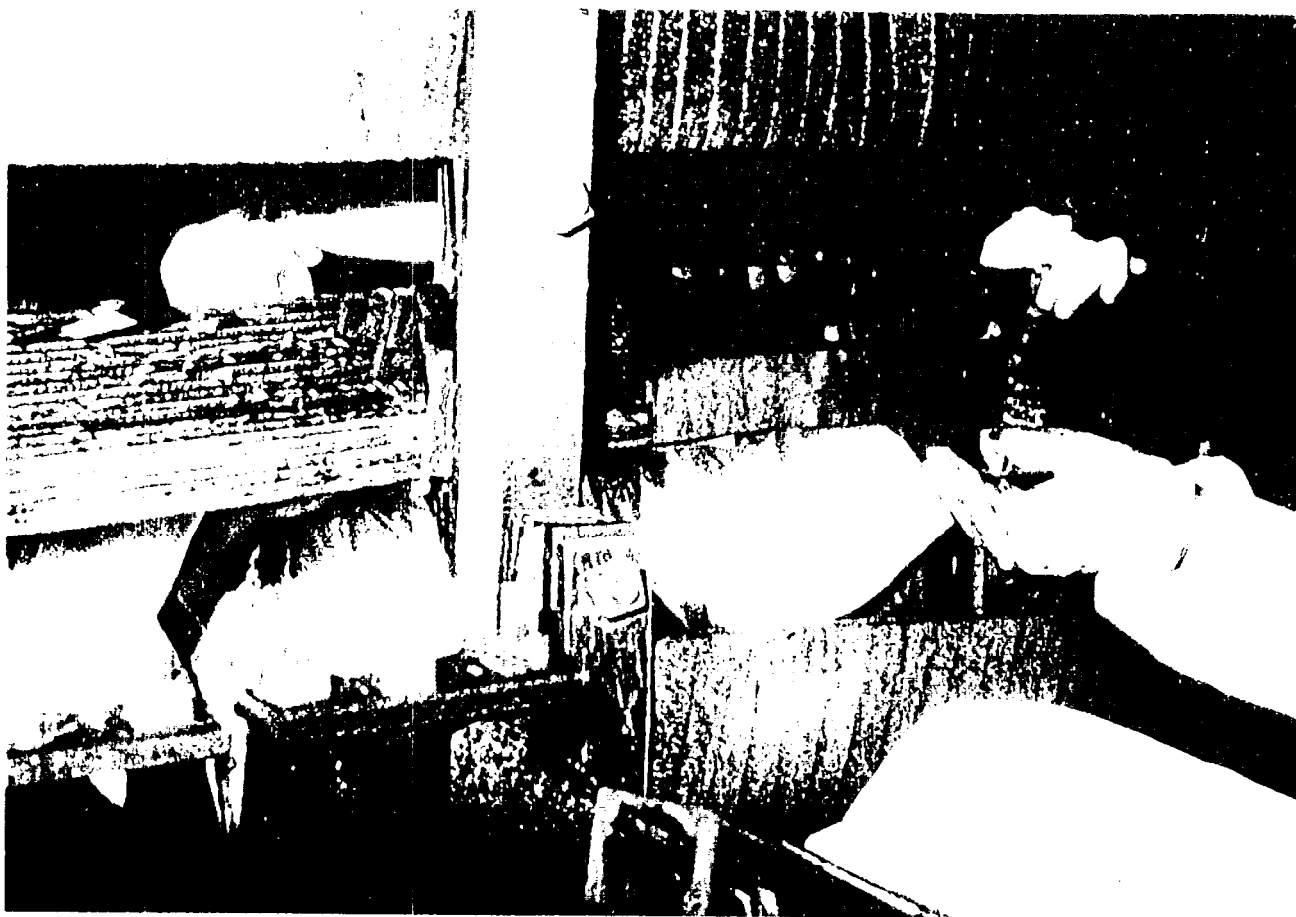
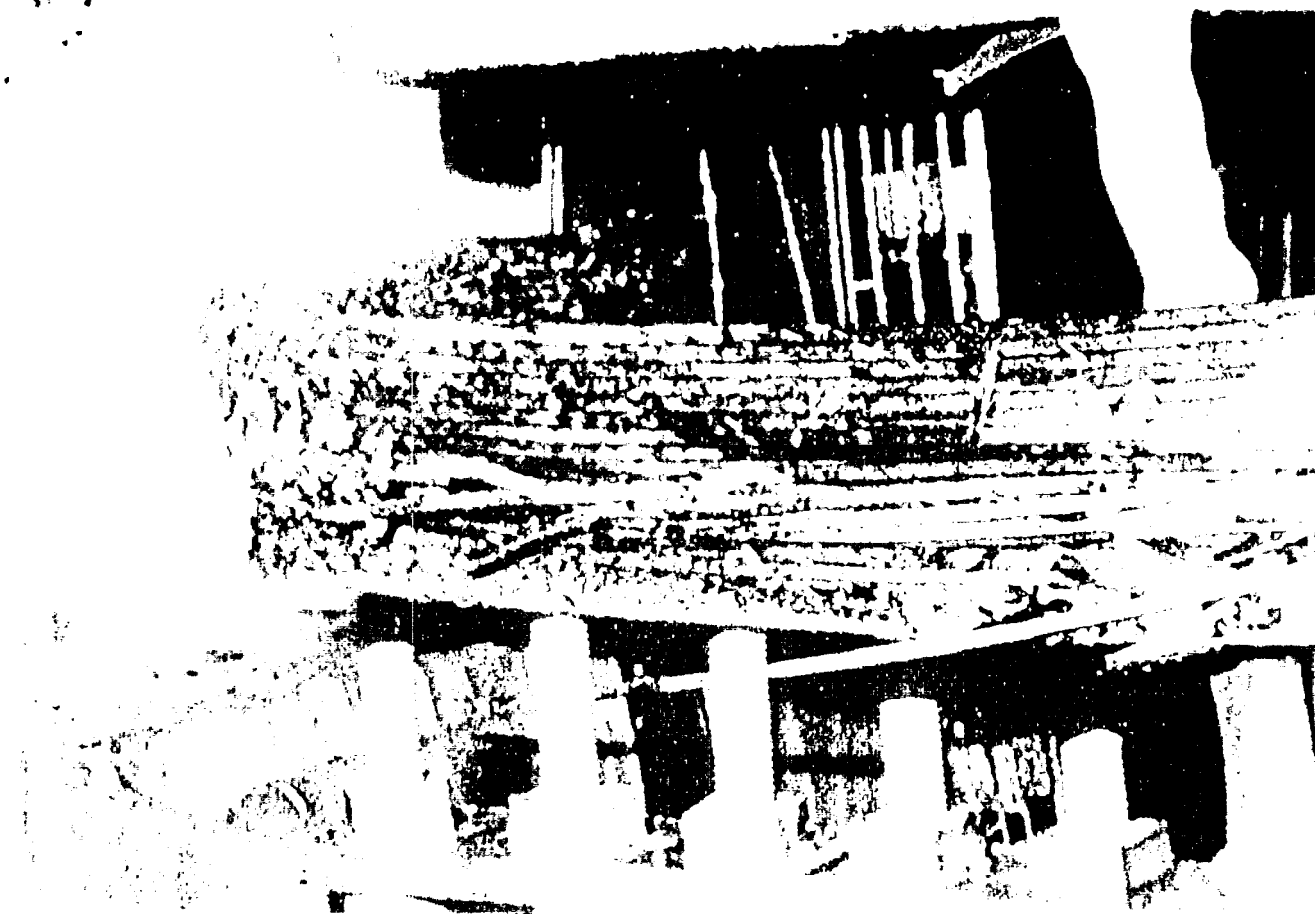
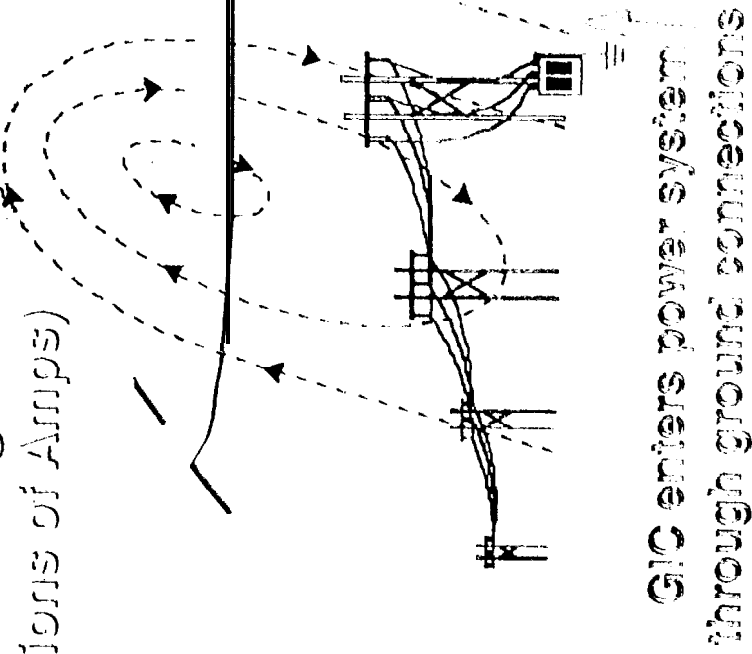


Figure 16

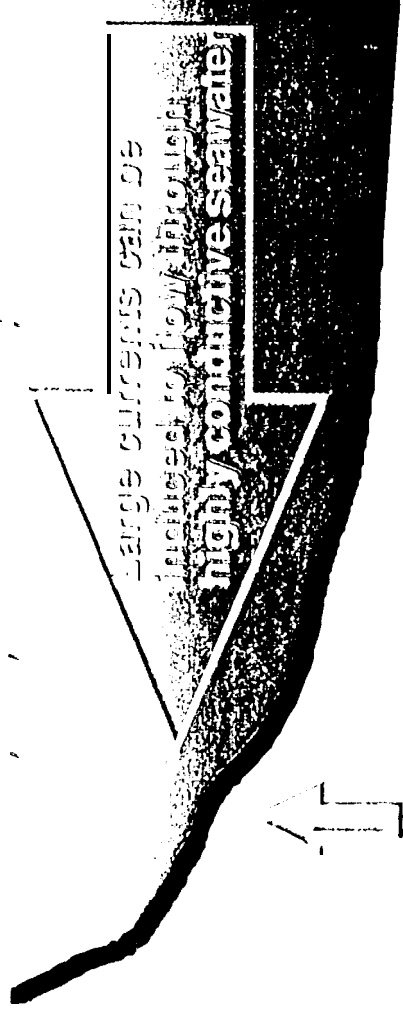
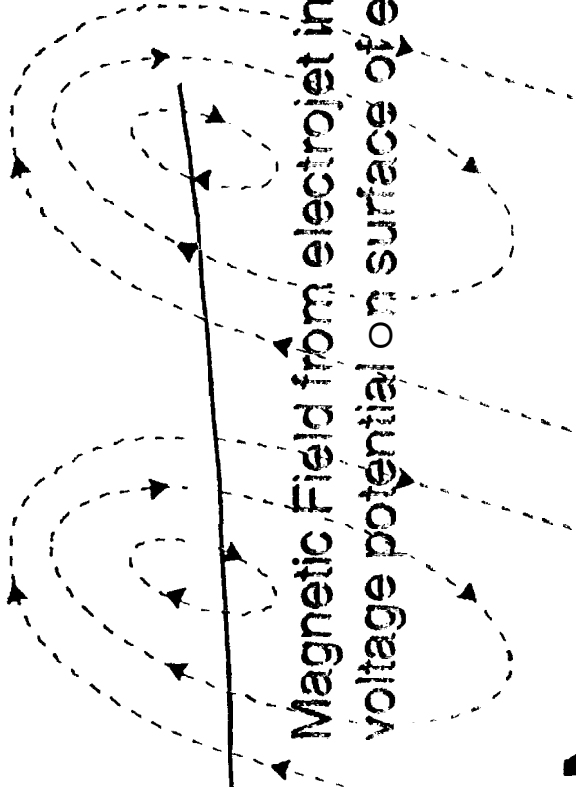
Fluctuating Electrojet (Millions of Amps)



Voltage Gradient



Magnetic Field from electrojet induces voltage potential on surface of earth



Coastal areas cause abrupt transition in conductivity between resistive rock geology and seawater

Electric potential induced on earth surface up to 5 Volts/km causes Geomagnetically Induced Currents

Figure 17